Electron localization–delocalization transitions in dissociation of the C_4^- anion: A large-*D* analysis

Qicun Shi and Sabre Kais[a)]
Department of Chemistry, Purdue University, West Lafayette, Indiana 47907

Dudley R. Herschbach[b)]
Department of Chemistry and Chemical Biology, Harvard University, Cambridge, Massachusetts 02138

(Received 5 September 2003; accepted 7 November 2003)

We present a study, employing high level *ab initio* methods, of electron localization–delocalization transitions along the dissociation path of the C_4^- anion to C_2 and C_2^-. We find that at the equilibrium geometry, the symmetrical and nonsymmetrical configurations of the linear C_4^- anion are almost isoenergetic. However, along a collinear dissociation path, the dipole moment drops abruptly to zero when the separation between the two middle carbon nuclei reaches about $R=2.15$ Å. The dipole moment remains zero until about $R=2.78$ Å, and then continuously increases as dissociation proceeds. This behavior is analogous to critical phenomena: The abrupt drop to zero of the dipole moment resembles a first-order phase transition, the later steady rise resembles a continuous phase transition. We show that a simple sub-Hamiltonian model, corresponding to the large-dimension limit for an electron in the field of four collinear carbon atoms, exhibits both kinds of phase transitions along the dissociation path. © *2004 American Institute of Physics.*
[DOI: 10.1063/1.1637581]

I. INTRODUCTION

Electron localization–delocalization transitions have a long history and remain a prime focus for both experimental and theoretical research.[1] This phenomenon was studied by Anderson who showed that an electron diffuses over only a finite length in one dimension in the presence of an arbitrary disorder potential.[2] Subsequently, a scaling theory was developed to investigate this transition and related localization problems.[3,4] This transition was also observed in solids,[5] liquids,[6] quantum Hall systems,[7] semiconductor super-lattices,[8] surface plasmons in nanosystems,[9] quasiperiodic driven systems,[10] quantum dots,[11,12] and in the tris-(2,2′-bipyridine)ruthenium(II) complex.[13] Here, we examine electron localization–delocalization transitions along the dissociation path of the C_4^- anion to C_2 and C_2^-.

Many theoretical studies have treated electronic structure and thermodynamic properties of the C_4 molecule;[15–20] these have been extensively reviewed.[21–23] Most experimental and theoretical work on C_4 has determined that the linear cumulene, with two unpaired electrons in a $3\sigma_g^2 3\sigma_u^2 4\sigma_g^2 1\pi_u^4 4\sigma_u^2 5\sigma_g^2 1\pi_g^2$, $^3\Sigma_g^-$ ground state, and the cyclic rhombic structure, with all electrons paired in a ^1A_g ground state, are nearly isoenergetic.[22] Bartlett *et al.* performed large scale calculations on C_4 using coupled-cluster singles, doubles and triples, CCSD(T), with a large basis set.[14] The rhombic isomer was found to be preferred by about 1 kcal/mole. Using *ab initio* calculations: Hartree–Fock (HF) and fourth-order perturbation theory MP4, Raghavachari showed that for the C_4^+ cation, like the neutral molecule, the linear chain and a rhombic isomer are nearly isoenergetic.[24] However, using multireference configuration interaction, Hogreve found that the carbon tetramer dication C_4^{2+} is metastable.[25]

Experiment and theory have confirmed that the structure of the C_4^- anion is linear with a $3\sigma_g^2 3\sigma_u^2 4\sigma_g^2 1\pi_u^4 4\sigma_u^2 5\sigma_g^2 1\pi_g^3$, $^2\Pi_g$ ground state.[14,22] Bartlett *et al.*, using large scale coupled-cluster calculations, found that the linear is lower than the cyclic structure by more than 30 kcal/mol.[14] For linear C_4^- the terminal bonds are predicted to be shorter than the central bond, which is opposite to what is found for the neutral C_4 molecule. All theoretical calculations[26,27] and experiments[28,29] have predicted that C_4^{2-} is metastable with a short lifetime, about 0.7 fs.[29]

In this paper, we study critical phenomena associated with electron localization–delocalization transitions along the dissociation path of the C_4^- anion. After describing, in Sec. II, the computational methods and geometry optimization used for C_4^-, we investigate in Sec. III the variation of the dipole moment along the dissociation path. In Sec. IV we show similar critical behavior can be obtained from a sub-Hamiltonian model representing the large-dimension limit for an electron in the field of four collinear carbon atoms. In Sec. V, we emphasize the semiclassical character of the large-dimension limit, and the general correspondence of symmetry breaking at $D\rightarrow\infty$ with electron–delocalization transitions at $D=3$.

II. COMPUTATIONAL METHODS AND GEOMETRIES

Our initial calculations employed the unrestricted Hartree–Fock (UHF) method, followed by high level *ab initio* correlated methods, including configuration interaction with singles and doubles (QCISD) and coupled clusters

a)Electronic mail: kais@power1.chem.purdue.edu
b)herschbach@chemistry.harvard.edu

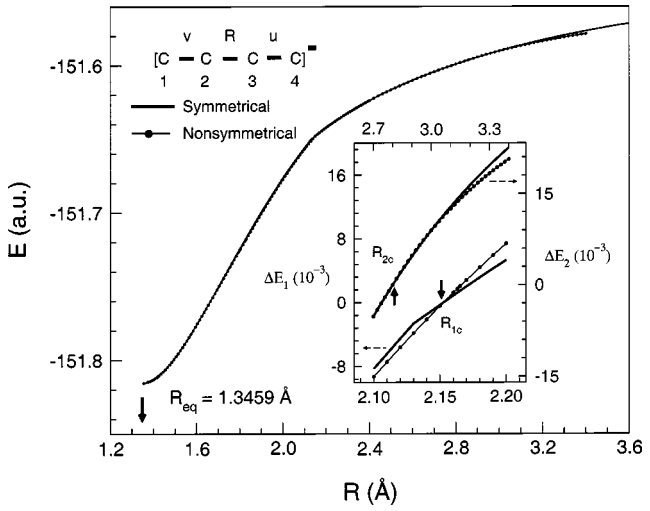

FIG. 1. Potential energy, obtained from QCISD with the 6-311+G(d) basis set, along collinear dissociation path of the C_4^- anion leading to C_2 plus C_2^-. The solid curve pertains to the symmetrical configuration ($v=u$), the dots to the nonsymmetrical configuration ($v\neq u$). Terminal bond distances v and u were optimized at each R. The inset shows the two critical points R_{1c} and R_{2c} where $\Delta E_1=E(R)-E(R_{1c})$ and $\Delta E_2=E(R)-E(R_{2c})$. ΔE is given in atomic units.

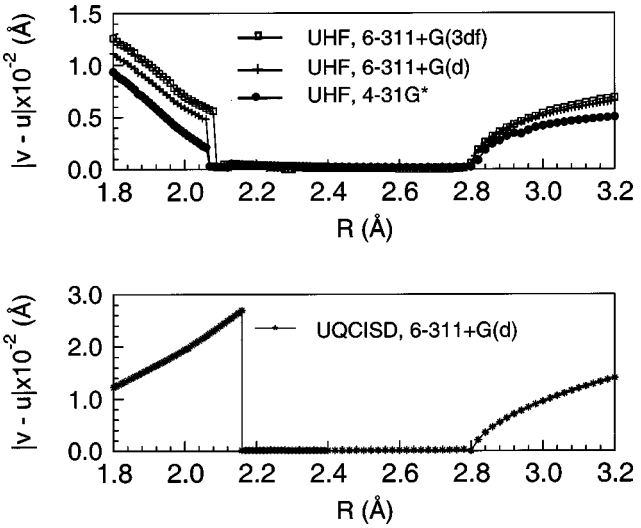

FIG. 2. Asymmetry parameter $|v-u|$ as a function of the dissociation coordinate R of the C_4^- anion, obtained from Hartree–Fock (UHF) calculations with different basis sets (upper panel) and from configuration interaction (UQCISD) with single and double excitations (lower panel). Terminal bond distances v and u were optimized at each R.

(CCSD). In all the calculations, we examined the effect of changing basis sets using the GAUSSIAN98 suite of programs.[30] The 6-311+G(d) basis set proved sufficient to describe the characteristics of the C_4^- anion. We first reexamined the structure of C_2^- and C_3^-. We found that in their optimized geometries the charge distributions are symmetrical no matter what initial guess for the geometry was tried. However, as seen in Fig. 1, geometry optimization of the linear C_4^- anion showed that the nonsymmetrical nuclear configuration (with $v\neq u$) is almost isoenergetic with the symmetrical one (with $v=u$). In all previous *ab initio* calculations the C_4^- anion was assumed to be symmetrical.[14,22] Table I compares the symmetrical and nonsymmetrical optimized configurations at the UHF, UCCSD, and UQCISD level of approximation. For all the optimized structures we carried out vibrational analysis to confirm that all the harmonic frequencies are real numbers. The differences in both energy and bond lengths are very small, but the UCCSD and UQCISD results consistently indicate that the symmetrical form is lower at the equilibrium geometry.

Figure 1 plots the potential energy along the collinear dissociation coordinate R, with v and u optimized at each distance R. At the optimized geometry corresponding to the equilibrium R, denoted by R_{eq}, the separation between the symmetrical and nonsymmetrical forms is only a few cm^{-1}, barely at the edge of numerical accuracy for the calculation. As R increases slightly above R_{eq}, the nonsymmetrical form very soon becomes lower in energy. We do not consider this a phase transition like those at R_{1c} and R_{2c} (shown below) because this switch occurs well within a ground-state vibrational amplitude. In this region near R_{eq} we may expect the actual molecule suffers breakdown of the Born–Oppenheimer approximation; the electronic and nuclear motions are no longer separable.

Simons[31,32] has shown that molecular anions possessing excess internal vibrational or rotational energy can lose their extra electron through radiationless transitions involving non-Born–Oppenheimer coupling. We considered electron detachment during vibrational motion of C_4^- as well as all possible fragmentation channels, and found that $C_4^-\rightarrow C_2+C_2^-$ is the energetically favored fragmentation channel.[33] As the dissociation coordinate R increases away from its equilibrium value, with the terminal bond lengths v and u optimized along the path, the nonsymmetrical form almost immediately becomes lower in energy, as seen in Fig. 1. Between $R_{1c}=2.15$ Å and $R_{2c}=2.78$ Å, however, the lowest energy form of the anion becomes symmetrical. For $R>R_{2c}$ the lowest energy form is again nonsymmetrical. In Fig. 2 we show the variation of the asymmetry parameter

TABLE I. Equilibrium geometry and energy of C_4^- obtained from *ab initio* methods.

Method[a]	Symmetry	E (a.u.)	$v=r_{12}$ (Å)	R (Å)	$u=r_{34}$ (Å)
UHF	Sym	−151.309 999 5	1.256 057 88	1.335 024 11	
	Nonsym	−151.310 026 5	1.256 041 84	1.335 044 63	1.256 031 86
UCCSD	Sym	−151.812 975 9	1.282 329 17	1.345 752 4	
	Nonsym	−151.812 974 6	1.282 218 38	1.345 710 04	1.282 425 86
UQCISD	Sym	−151.815 624 7	1.283 999 68	1.345 900 88	
	Nonsym	−151.815 623 3	1.284 025 9	1.345 885 99	1.283 995 12

[a]In each case the 6-311+G(d) basis set was used.

$|v-u|$ as a function of R using both UHF theory with different basis sets and the UQCISD method. The abrupt change between symmetrical and nonsymmetrical forms at R_{1c} resembles a ''first-order'' phase transition, the steady rise that sets in at R_{2c} resembles a ''continuous'' or ''second-order'' phase transition.

Usually wave functions obtained from mean-field theory need not obey the invariances present in the full Born–Oppenheimer Hamiltonian. A common manifestation of this ''symmetry dilemma'' is found where variationally optimal spin restricted and unrestricted open shell Hartree–Fock wave functions often do not transform as pure irreducible representations of the molecular point group for nondegenerate electronic states, a phenomenon which has been termed ''artifactual symmetry breaking'' by Davidson and Borden.[34] The manifestation of this phenomenon has been discussed extensively in the literature for a number of molecules.[34–39]

The ground state of C_4^- anion is linear with a $^2\Pi_g$ symmetry. The computational point group $D_{\infty h}$ allows π_x to become different than π_y; this particular type of spatial symmetry breaking is common for linear molecules and is not generally considered to be a significant problem.[37,40] It has been found empirically that breaking inversion symmetry is much more serious; this lowers the wave function symmetry from $D_{\infty h}$ to $C_{\infty v}$. We have checked the symmetry breaking near the equilibrium geometry using UHF, UQCISD, and UCCSD. Taking the equilibrium geometry of the UCCSD results as a reference, we checked each of the symmetrical and nonsymmetrical energies (UHF, UQCISD, UCCSD) as a function of the asymmetry stretching coordinate. The energy differences are defined as

$$\Delta E = E_{D_{\infty h}}(r=r_1=r_2) - E_{D_{\infty h}}(r_1=r_2=r_{\mathrm{eq}}),$$

$$\Delta R = r_{\mathrm{eq}} - r, \tag{1}$$

with $\Delta E(-x)=\Delta E(x)$ for the symmetrical solution, and for the nonsymmetrical one

$$\Delta E = E_{C_{\infty v}}(r=r_1) - E_{C_{\infty v}}(r_2=r_{\mathrm{eq}}), \quad \Delta R = r - r_{\mathrm{eq}}, \tag{2}$$

$$\Delta E = E_{C_{\infty v}}(r=r_2) - E_{C_{\infty v}}(r_1=r_{\mathrm{eq}}), \quad \Delta R = r_{\mathrm{eq}} - r. \tag{3}$$

In order to understand the artifactual symmetry breaking, we have followed Gwaltney and Head-Gordon[35] by plotting the energies of the three solutions to the self-consistent field (SCF) equations in the left panel of Fig. 3. The vertical axis is the energy difference with respect to the symmetric solution at equal bond lengths and the horizontal axis is the antisymmetric stretch coordinate. This plot exhibits the symmetry dilemma of the Hartree–Fock theory: Do we have to follow the higher energy curve which possesses correct symmetry at $D_{\infty h}$ geometry, or the lower energy curves which do not.[41] In Fig. 3 we present also the UCCSD and UQCISD curves corresponding to the three UHF solutions. The two solutions now lie much closer but we still see the unphysical existence of artifactual states. Moreover, we extended the calculations to include the Bruecker-orbital coupled cluster doubles method (BDT), which is commonly used to eliminate the artifactual symmetry breaking problem.[35] At the equilibrium geometry, the symmetrical structure is lower in energy (by 0.001 07 a.u.) compared with the nonsymmetrical form. However, along the dissociation path, $R_{\mathrm{eq}}<R\leqslant R_{1c}$, the nonsymmetrical is lower in energy. Moreover, all the five harmonic frequencies for both the symmetrical and nonsymmetrical are real and in good agreement with the experimental results as shown in Table II. Density-functional calculation, using Becke three (B3LYP) functional, give very similar results. The nonsymmetrical and symmetrical energy difference at the equilibrium geometry is $-0.000\,02$ a.u. or -0.014 kcal/mol. The density-functional results are consistent with the *ab initio* results.

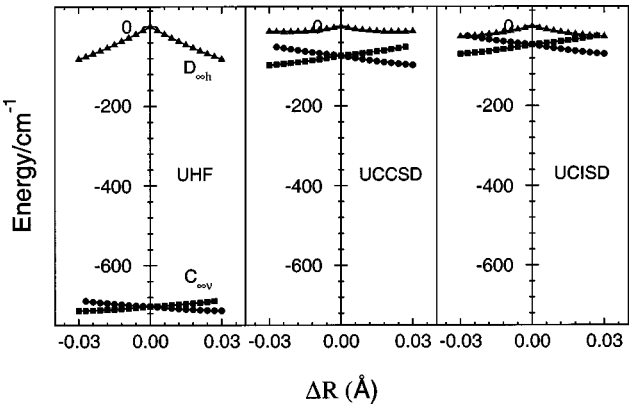

FIG. 3. UHF, UCCSD, and UQCISD energies around the C_4^- anion minimum geometry as a function of the antisymmetyric stretch coordinate.

At the nonsymmetrical equilibrium geometry, UQCISD results show that the spin contamination is $S^2=0.7516$ compared to $s(s+1)=0.75$ for the ground state $^2\Pi_g$ of C_4^- with $s=1/2$. In the range 1.4 Å$<R<R_{1c}$ the $S^2\approx 0.75$ but close to the critical point $R_{1c}=2.16$ Å the value of S^2 jumps to a higher value $S^2\approx 5.5$ which indicates that some other spin state is mixed in. However, it is important to mention that for

TABLE II. Vibrational frequencies (in cm^{-1}) for symmetrical (SY) and nonsymmetrical (NS) forms of C_4^- anion.

	UBD(T)		UB3LYP		
f(vib.)	NS	SY	NS	SY	Expt. (Refs. 53 and 54)
$\nu_1(\sigma_g)$	2053.7	2060.9	2098.6	2098.2	2047(20)
$\nu_2(\sigma_g)$	890.3	888.9	919.4	919.2	936(20)
$\nu_3(\sigma_u)$	1702.0	1705.5	1768.9	1768.7	1699.8
$\nu_4(\pi_g)$	311.0/255.8	346.7/268.1	507.2/439.2	504.4/434.8	396(20)
$\nu_5(\pi_u)$	211.4/193.7	200.5/198.7	241.7/221.3	239.6/218.9	

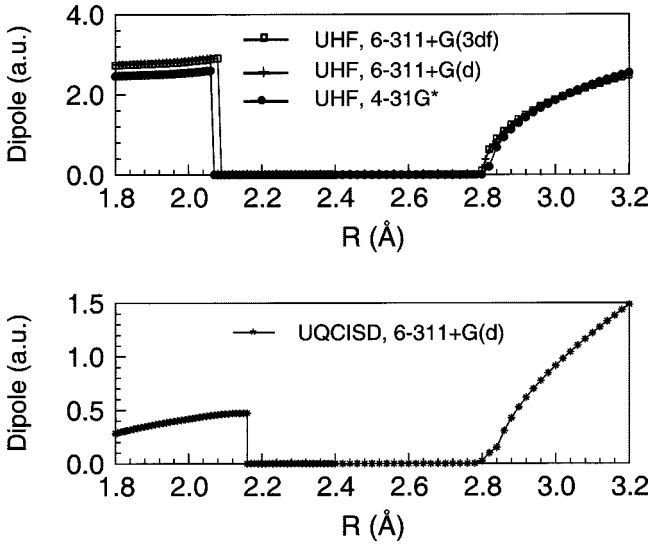

FIG. 4. Dipole moment of the linear C_4^- anion as a function of the distance R, obtained from both UHF and UQCISD approximations, as in Fig. 2. Terminal bond distances v and u were optimized at each R. The origin for the dipole moment is midway between the two central carbon nuclei. [Note: 1 dipole a.u. (Bohr−Electron)=2.54 Debye].

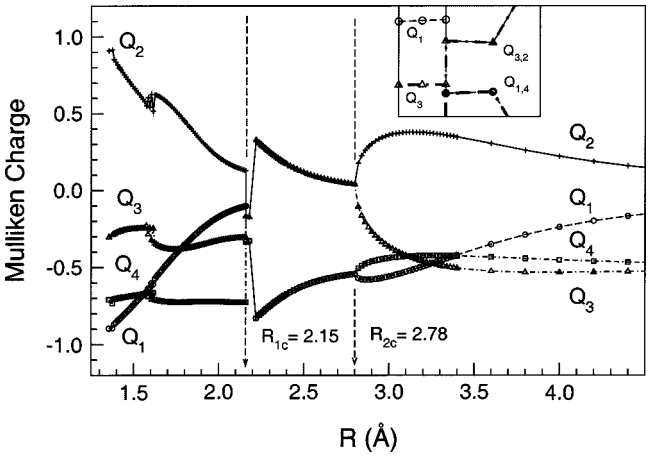

FIG. 5. Mulliken charges $Q_i(R)$ along the collinear dissociation path for C_4^-. R_{1c} and R_{2c} values are marked with vertical dashed lines. Note how the $Q_i(R)$ vary strongly outside the band between R_{1c} and R_{2c} and near R_{1c} (see upper inset), whereas within the band $Q_1=Q_4$ and $Q_2=Q_3$, thus making very clear the origin of the behavior seen in Fig. 4.

$R>R_{1c}$ we follow the symmetrical solution with $D_{\infty h}$ symmetry.

Because we evaluated the energy at points closely spaced in R, it was feasible to determine the critical exponent for the continuous transition by expanding the difference of the UQCISD energies, $\Delta E=E^{\mathrm{sym}}-E^{\mathrm{nonsym}}$, about the critical radius, R_{2c}. This gave

$$\Delta E=a+b(R-R_{2c})+c(R-R_{2c})^{\beta}+\cdots, \tag{4}$$

the best-fit values obtained for the coefficients were (in microhartree units): $a=86.7$; $b=-677.5$; $c=1931.5$; the exponent $\beta=2.06$, which is close to the value 2 corresponding to a mean-field approximation.[42] The nonzero value of the a-coefficient is a measure of the errors in energies given by the Gaussian program and the fitting procedure. When the data were fit with the constraint $b=0$, we obtained $a=9.4$, $c=1319.6$, and $\beta=2.58$; as the error becomes smaller, this fit is appreciably better and thus indicates the exponent β is significantly larger than the mean-field value.

III. DIPOLE MOMENT ALONG DISSOCIATION PATH

The transitions between symmetrical and nonsymmetrical forms for the ground state seen in Figs. 1 and 2 have a direct effect on the dipole moment. Figure 4 shows the variation of absolute values of the calculated dipole moment along the collinear dissociation path. Much as in Fig. 2 for the asymmetry parameter, the dipole moment drops abruptly to zero at $R_{1c}=2.15$ Å, remains zero up to $R_{1c}=2.78$ Å, and thereafter rises steadily to infinity as the dissociation fragments separate. An expansion of the UQCISD results for the dipole moment analogous to Eq. (4) with $b=0$ gave (in atomic units) $a=-0.06$; $c=1.88$; and $\beta=0.69$, or $\sim 2/3$. The same expansion of the Hartree–Fock results, representing the mean-field approximation, gave values of β near 1/3, increasing from 0.35 up to 0.4 as the basis sets used became larger. The difference between the UQCISD and UHF results, which appears large enough to be significant, indicates that electron correlation substantially affects the critical exponent for the dipole moment transition.

Some insights into the dramatic changes seen in the dipole moment can be obtained by examining how the corresponding Mulliken charge distributions[43] vary with R, as shown in Fig. 5. The dipole moment is zero when the charge distribution is symmetrical, as at $R=2.4$ Å, but nonzero for nonsymmetrical charge distributions. At a large distance, such as $R=4.5$ Å, the charge distribution has nearly separated into that for the neutral C_2 and the anion C_2^-; for the latter, the Mulliken charges are close to $-1/2$ and $R_{\mathrm{eq}}=1.2797$ Å is notably shorter than the length of a terminal bond in the C_4^- anion.

Interestingly, the Mulliken charges suggest the dipole moment at the equilibrium distance, $R_{\mathrm{eq}}=1.346$ Å, should be nonzero. There the symmetrical form, which has zero dipole, is very slightly lower in energy than the nonsymmetrical form, which has $\mu=1.64\times10^{-4}$ a.u., and $|u-v|=5.54\times10^{-5}$ a.u. However, as noted above, as R increases slightly above R_{eq}, the nonsymmetrical form becomes the lower one and the dipole moment begins to increase appreciably. This situation allows the Mulliken charges to be nonsymmetrical; at R_{eq} the values are $Q_1=-0.90$; $Q_2=0.93$; $Q_3=-0.31$; and $Q_4=-0.71$. As the dipole moment involves the product of charge and distance, integrated over the charge distribution and weighted by the volume element, a point charge model has difficulty simulating behavior when asymmetries in the distributions of charge and spatial positions distributions are shifting rapidly.

Comparing the ordinate scales for Figs. 2 and 4 indicates that only a small part of the change in dipole moment comes from the difference in the terminal bond lengths. Most of the variation in the dipole moment thus must result from the shift of the center of charge relative to the origin, which is taken midway between the central pair of carbon atoms. This aspect is readily examined using the Mulliken charges. For

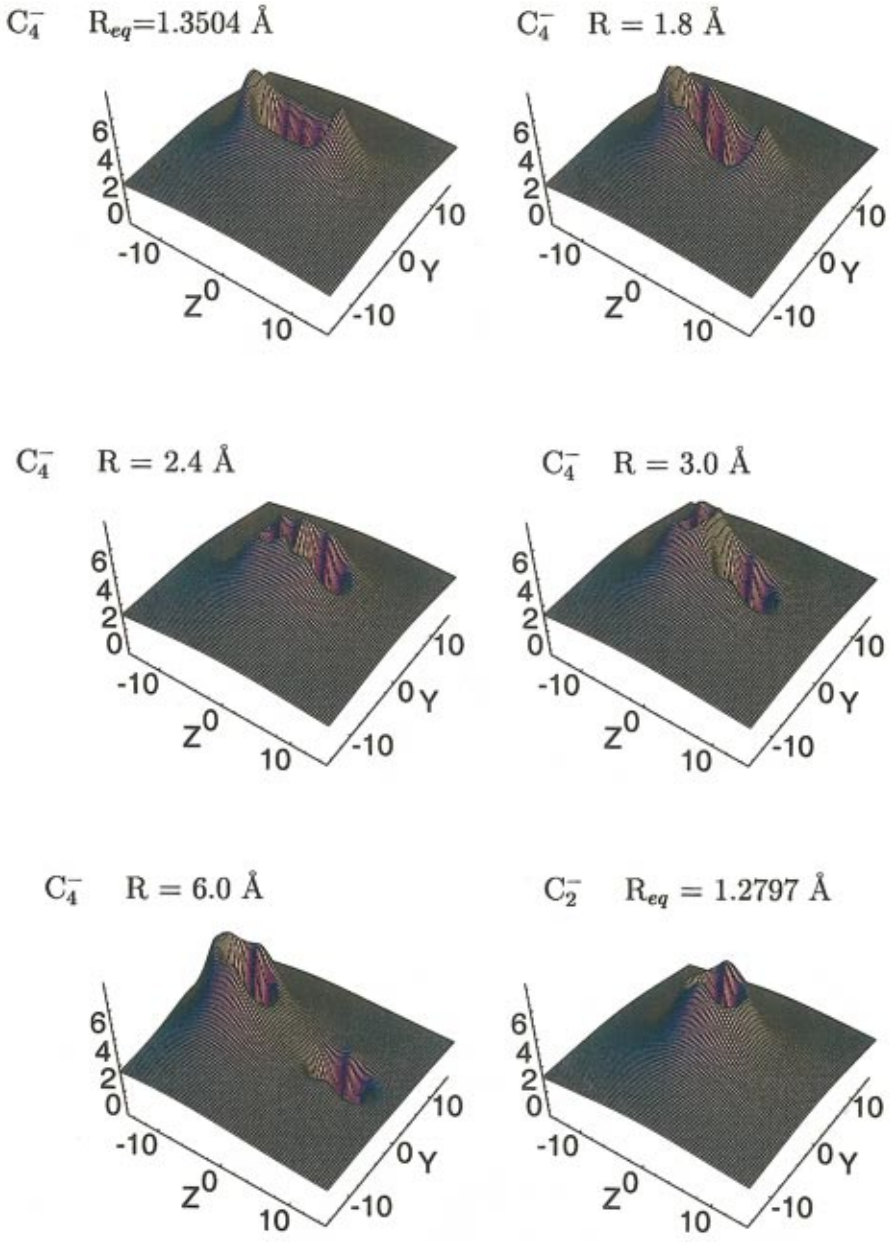

FIG. 6. (Color) Contour plots of the electrostatic potential for the C_4^- anion, defined in Eq. (1), vs z (in Å; along internuclear axis, origin midway between two central carbon nuclei) and y (in Å; coordinate perpendicular to internuclear axis), for different values of R along the dissociation path. For comparison a plot for C_2^- at its equilibrium internuclear distance is included at lower right.

four collinear charges Q_i along the z axis, the dipole moment is simply given by $\mu=\Sigma_i Q_i\, z_i$; then with the two terminal C–C lengths v, u and the middle C–C distance R, we have

$$\mu = Q_1\left(-\frac{R}{2}-v\right)+Q_2\left(-\frac{R}{2}\right)+Q_3\left(\frac{R}{2}\right)+Q_4\left(\frac{R}{2}+u\right)$$
$$=\mu_1+\mu_2, \tag{5}$$

with

$$\mu_1=\frac{R}{2}(-Q_1-Q_2+Q_3+Q_4), \quad \mu_2=Q_4u-Q_1v. \tag{6}$$

Thus, μ_1 arises from the displacement of the center of charge from the origin, μ_2 from any difference in the charges on the terminal atoms or asymmetry in the terminal bond distances. With the atoms numbered as in Fig. 4, when R becomes sufficiently large, $Q_1=Q_2\sim 0$, and $Q_3=Q_4\sim -1/2$; hence $\mu_1\sim -R/2$ and $\mu_2\sim -u/2$ and the total $\mu\sim -(R+u)/2$, which is just the dipole moment of C_2^- as measured from the origin. Even for modest $R>R_{2c}$, typically $|\mu_1|$ is much larger than $|\mu_2|$. For example, at $R=3$ Å, we see from Fig. 5 that $Q_1\approx Q_3\approx Q_4\approx -1/2$; $Q_2\approx +1/2$ and thus Eq. (6) gives $\mu_1\approx -R/2=-2.8$ a.u. and $\mu_2\approx -(u-v)/2=-0.02$ a.u., roughly in agreement with the UHF result of Fig. 4. As R approaches R_{2c} from above, in Fig. 5 we find $Q_1+Q_2\approx Q_3+Q_4$ with $Q_2\approx Q_3$ and $u\approx v$; these relations become exact for the approach from below. Thus, Eq. (6) requires that just above the critical point μ_1 becomes very small because the Mulliken charges nearly cancel whereas μ_2 becomes small because the terminal bond distances approach equality. Even for this simple model, these different dependences of μ_1 and μ_2 cause the total dipole to mimic the small kink and curvature just above R_{2c} that are seen in the UQCISD results of Fig. 4.

Figure 6 displays the variation along the dissociation

path for another property, related to the dipole moment. This is the electrostatic potential for C_4^-, which is defined as

$$V(r)=\sum_{\alpha=1}^{K}\frac{Z_\alpha}{|r-r_\alpha|}-\sum_{i=1}^{N}\int\frac{\phi_i^*\phi_i}{|r-r_i|}d\tau. \tag{7}$$

The first term describes the electrostatic repulsion between the $K=4$ carbon nuclei and the probing charge while the second term corresponds to the electrostatic attraction between the probing charge and the $N=25$ electrons in the molecular orbitals (ϕ_i) of the C_4^- anion.

The peaks appearing in the contour plots in Fig. 6 indicate the relatively high concentration of the extra electron charge -1. At equilibrium, the distribution of the potential of the anion felt by a negative probing charge is symmetrical. Thus the extra electron could be on either side of the C_4 molecule. As the distance along the dissociation path increases, between R_{1c} and R_{2c} the electron moves to the center. However, at larger distances exceeding about $R=6$ Å, the electron shifts completely to one side and the electrostatic potential looks like that for the C_2^- anion as shown in the lowest panel of Fig. 6.

IV. MODEL FOR LARGE-DIMENSIONAL LIMIT

Dimensional scaling theory[46] provides a natural means to examine electron localization–delocalization transitions. At the large-dimension limit ($D\to\infty$), in a suitably scaled space electrons become fixed in position but their geometrical configuration typically undergoes marked changes for certain ranges of the nuclear charges[44] or molecular geometry.[45,46] Recently, the symmetry breaking of electronic structure configurations at the large-D limit has been shown to be completely analogous to phase transitions and critical phenomena in statistical mechanics.[47–50] Because the large-D limit is pseudoclassical, the analysis deals with a point charge representation rather than a differential equation; thus, energies are obtained simply by finding the minimum of a scalar effective potential. However, the previous treatments of phase transitions[47–50] dealt only with two-electron atoms and one- or two-electron diatomic molecules. In order to carry out an analogous treatment for the C_4^- anion, with 25 electrons, we employ a sub-Hamiltonian method developed by Loeser.[51,52] We find this provides an explicit demonstration of the two kinds of transitions found at $D=3$ along the dissociation path of the C_4^- anion to C_2 and C_2^-.

Loeser's method[51] provides a systematic procedure to construct large-D limit Hamiltonians that are internally modified to reflect major finite-D effects. These functions, termed sub-Hamiltonians, are obtained by scaling the kinetic terms represented by generalized centrifugal potentials at the $D\to\infty$ limit. As applied to molecules, the method considers the nuclear framework to be fixed and strictly three-dimensional, in accord with the Born–Oppenheimer approximation. For our purpose, it is sufficient to consider the simplest sub-Hamiltonian variant;[52] this employs the Hartree–Fock approximation and has the form

$$\mathcal{H}=\sum_i\frac{n_i^2}{2r_{n_i}^2}+\frac{1}{2}\left(\sum_I\sum_J\frac{Z_IZ_J}{R_{IJ}}-\sum_I\sum_j\frac{Z_I}{R_{Ij}}+\sum_i\sum_j\frac{1}{R_{ij}}\right). \tag{8}$$

The first term arises from a hydrogenic scaling of the centrifugal potential, where n_i are the atomic principal quantum numbers and r_{n_i} are radii associated with the corresponding shells. The other terms comprise the Coulombic interactions among the electrons and nuclei, involving distances defined by

$$\begin{aligned}R_{IJ}&=((x_I-x_J)^2+(y_I-y_J)^2+(z_I-z_J)^2)^{1/2},\\ R_{Ij}&=((x_I-x_j)^2+(y_I-y_j)^2+(z_I-z_j)^2+r_{n_j}^2)^{1/2},\\ R_{ij}&=((x_i-x_j)^2+(y_i-y_j)^2+(z_i-z_j)^2+r_{n_i}^2+r_{n_j}^2)^{1/2},\end{aligned} \tag{9}$$

with I,J indices for nuclei and i,j for electrons. Here the x,y,z coordinates pertain to the ordinary $D=3$ subspace, whereas the radii r_{n_i} of the electron shells also contain $D-3$ auxiliary components specifying projections outside of and perpendicular to the x,y,z subspace. These "extra" components simulate the effects of quantum mechanical delocalization within the localized representation of the sub-Hamiltonian.

In the simplest level of approximation, the degrees of freedom for the electrons within x,y,z space can be eliminated by fixing those spatial coordinates to coincide with those of the nearest nucleus; this corresponds to omitting polarization effects.[52,51] The sub-Hamiltonian for the linear C_4^- cation then can be written as $H=H_s+H_e$, where the 24 shell electrons appear in

$$H_s=\sum_{I=1}^{4}\sum_{s=1}^{2}\frac{N_{Is}n_s^2}{2r_{Is}^2}+\frac{1}{2}\left(\sum_{I,J=1}^{4}\sum_{s=1}^{2}\frac{Z_IN_{Js}}{R_{I,Js}^2}+\sum_{I,J=1}^{4}\sum_{s,t=1}^{2}\frac{N_{Is}N_{Jt}}{R_{Is,Jt}}\right). \tag{10}$$

Here n_s denotes the shell quantum number; N_{Is} the number of electrons in shell s about nucleus I; indices s and t designate either of the two shells $n=1$ (with 2 electrons) or $n=2$ (with 4 electrons) of each carbon atom. The shell radii r_{Is} now contain just the $D-3$ auxiliary components; the distance $R_{I,Js}$ between a nucleus I and a shell electron about another nucleus is

$$R_{I,Js}=((x_I-x_{Js})^2+(y_I-y_{Js})^2+(z_I-z_{Js})^2+r_{Js}^2)^{1/2}, \tag{11}$$

and the distances between intershell and intrashell electrons are

$$R_{Is,Jt}=((x_{Is}-x_{Jt})^2+(y_{Is}-y_{Jt})^2+(z_{Is}-z_{Jt})^2+r_{Is}^2+r_{Jt}^2)^{1/2}. \tag{12}$$

The four nuclei are arranged collinearly along the z-axis; thus $x_I=y_I=0$ and $z_I=-R/2-v;-R/2;R/2;R/2+u$, respectively, for $I=1,2,3,4$.

The 25th electron of the anion appears in

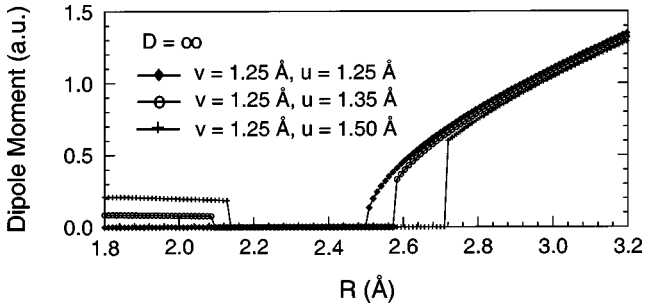

FIG. 7. The axial dipole moment at the large-D limit as a function of R (shifted by 1.82 Å) for an electron in the field of four collinear carbon atoms, with v fixed at $v=1.25$ Å and three values of u ($=1.25$, 1.35, and 1.5 Å).

$$\mathrm{H}_e=\frac{n_0^2}{2r_0^2}-\sum_{I=1}^{4}\left(\frac{Z_I}{R_{0I}}+\sum_{s=1}^{2}\frac{N_{Is}}{R_{0,Is}}\right), \tag{13}$$

where $n_0=2$; the radius r_0 contains the $D-3$ auxiliary components of the electron, but its z-component in 3-space is not required to coincide with that of any of the nuclei. The distance R_{0I} between the electron and nucleus I thus may be written as

$$R_{0I}=((z-z_I)^2+r_0^2)^{1/2}, \tag{14}$$

and the distance $R_{0,Is}$ between the lone electron and those in shell Is is given by

$$R_{0,Is}=(R_{0I}^2+r_{Is}^2)^{1/2}. \tag{15}$$

In the point charge representation provided by the sub-Hamiltonian formalism, the electronic symmetry actually is determined by the z-coordinate of the lone extrashell electron.

The energy of the sub-Hamiltonian $\mathrm{H}=\mathrm{H}_s+\mathrm{H}_e$ for any conformation of the nuclei, as specified by R, u, and v, is obtained by finding the global minimum as a function of ten variables: the eight r_{Is} (with $I=1-4$ and $s=1-2$) and r_0, z.

At the large-D limit the axial dipole moment, measured from the midpoint between the two central carbon nuclei, is given by the z-component of the vector

$$\boldsymbol{\mu}_\infty=\sum_{I=1}^{4}\left(Z-\sum_{s=1}^{2}N_{Is}\right)\mathbf{r}_{Is}-\mathbf{r}, \tag{16}$$

where the vector $\mathbf{r}$ denotes the location of the lone extrashell electron of Eq. (13); its magnitude is given by $(\rho^2+z^2)^{1/2}$, with ρ the perpendicular distance of the electron from the internuclear axis. In the simplistic approximation employed here, the shell electrons of Eq. (10) do not contribute to the dipole moment, because in Eq. (16) the coefficient of $\mathbf{r}_{Is}$ vanishes for each carbon atom (as $Z=6$, $N_{I1}=2$, $N_{I2}=4$). Accordingly, in this simplest sub-Hamiltonian model, the dipole moment is determined solely by $\mathbf{r}$, and thus must vanish whenever the lone electron lies in the plane midway between the two central carbon atoms (i.e., when $z=0$).

Figure 7 shows the variation of dipole moment with the distance R between the central carbon nuclei, as obtained from this large-D limit for fixed $v=1.25$ Å and different values of u ($=1.25$, 1.35, and 1.5 Å). Qualitatively, the simple sub-Hamiltonian model exhibits behavior similar to Fig. 4. However, the transition points, R_{1c} and R_{2c}, obtained from the global minimum of $\mathrm{H}_s+\mathrm{H}_e$ were found to be unrealistically small. Accordingly, in Fig. 7 we shifted the scale for R upwards by adding 1.82 Å, twice the average radius of a carbon atom. This adjustment emphasizes the crudeness of the point charge model but does not detract from its heuristic utility. Table III lists the corresponding values of R_{1c} and R_{2c} and the associated energies, obtained for choices of v and u equal to or near to those found from our *ab initio* UQCISD calculations.

In Fig. 7, the dipole moment is nearly constant for $R<R_{1c}$, before dropping abruptly to zero, then rising again for $R>R_{2c}$ and climbing steadily with concave curvature corresponding to $\beta=0.58$. The onset of the transition at $R>R_{2c}$ is gradual for $v=u$ but becomes abrupt for $v\neq u$, just as it does at R_{1c}. In most aspects, these features are remarkably similar to the *ab initio* results of Fig. 4, although the point charge model yields very poor estimates of the magnitude of the dipole moment. A major handicap for the model is the simplifying assumption adopted in Eq. (10); as noted, this eliminates any contributions from the 24 shell electrons in Eq. (16), so that the dipole moment arises only from the single extrashell electron.

Figure 8 displays energy contours for the sub-Hamiltonian of Eq. (13) pertaining to that electron, as R, v, and u are varied. These plots help elucidate two notable aspects of Fig. 7, wherein (i) the dipole moment is zero for R appreciably above R_{1c} even when $v\neq u$ there, and (ii) the dipole moment becomes nonzero for $R>R_{2c}$ even when $v=u$. In essence, the single extrashell electron is behaving in a way analogous to that in H_2^+. In region (i) the electron remains midway ($z=0$) between the middle two carbon atoms, even when distances to the terminal carbons differ. In region (ii), at larger R, the electron shifts to one of the separating pairs of carbon atoms (so $z>0$), even when the bond length is the same for both pairs. The actual transition at $R=R_{2c}$ occurs with $v=u$, after which the bond length of the

TABLE III. Transition point geometry and energy of C_4^- obtained from UQCISD method and from sub-Hamiltonian model.

Methods	v (Å)	u (Å)	R_{1c} (Å), E_{1c} (a.u.)	R_{2c} (Å), E_{2c} (a.u.)
UQCISD	1.2683	1.2947	2.15, −151.6480	
	1.2588	1.2591		2.78, −151.6003
sub-Hamiltonian	1.2683	1.2947	2.10, −129.5	2.55, −143.2
	1.2588	1.2688[a]	2.08, −128.3	2.54, −143.0

[a]Here, for purpose of comparison, u is chosen larger than v by 0.1 Å.

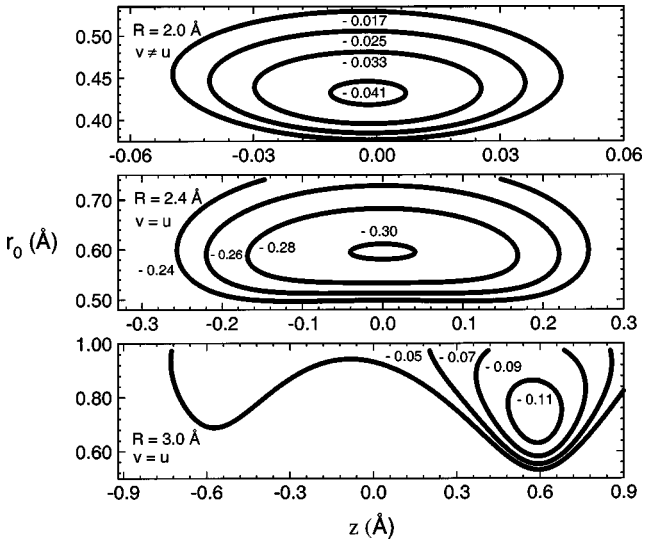

FIG. 8. Contour plots of energy (in a.u.) vs r_0 and z (in Å) of the extrashell electron by H_e of Eq. (13), with the eight variables r_{Is} (for $I=1$ to 4 and $s=1$ to 2) fixed at values giving the global minimum of H_s+H_e. The upper, middle and lower panels pertain to different internuclear distances $(v,u,R)=(1.25,1.35,2.0)$, (1.25, 1.25, 2.4), and (1.25, 1.25, 3.0), respectively.

C_2^- fragment exceeds that of the C_2 fragment (so $u>v$, for the labeling adopted in Fig. 1). The model is consistent with the second-order character of the transition at R_{2c}; with $v=u$, it is evident from Eqs. (13)–(15) that $H_e(\rho,z)=H_e(\rho,-z)$ is an even function of z, so a Taylor expansion about $z=0$ contains only even powers of z. Despite the drastic simplifications of the sub-Hamiltonian model, it does serve to exemplify that the charge distribution becomes symmetric for $R_{1c}<R<R_{2c}$ and nonsymmetric elsewhere, in accord with Fig. 5.

V. CONCLUDING REMARKS

Our *ab initio* calculations, using UHF, UQCISD, UCCSD with different basis sets, all exhibit the same critical phenomena: As we move outward along the collinear dissociation path, the dipole moment of C_4^- drops abruptly to zero at R_{1c}, remains zero up to R_{2c}, then becomes nonzero again and gradually climbs to infinity as $R\to\infty$. The abrupt drop at R_{1c} resembles a ''first-order'' phase transition, the sedate change that sets in at R_{2c} resembles a ''continuous,'' second-order phase transition. However, the complexity of such electronic structure computations renders them unsuitable for detailed study of the origin and character of the phase transitions.

The large-dimension limit offers a tractable approach. Although the $D\to\infty$ limit may appear arcane, it seems to capture the chief physical features of electron localization–delocalization behavior at $D=3$, as shown in several applications.[47–50] This likely stems from three aspects of dimensional scaling.[46] (1) When employed either for dimensional interpolation or perturbation expansions, the pertinent variable is $1/D$. Thus, in relation to other dimensions the large-D limit actually represents the origin $(1/D\to 0)$, substantially closer to the ''real world'' (at $1/D=1/3$) and therefore more realistic than are one-dimensional models (at $1/D=1$) of the kind customarily invoked. (2) When treating problems involving Coulombic interactions, the distance scale is taken proportional to D^2, hence the conjugate momenta are scaled as D^{-2} and thereby the uncertainty principle remains unaffected. Accordingly, although in the $D\to\infty$ limit the electrons are at rest in fixed positions in the scaled space, quantum fluctuations still occur as usual in the corresponding unscaled space. (3) The limit $D\to\infty$ is tantamount to swelling the electron mass to infinity or to shrinking Planck's constant to zero. Accordingly, this limit represents a semiclassical regime, but it is different in character from the more familiar Wentzel–Kramers–Brillouin (WKB) approximation. With D-scaling, the limit is taken in a way that converts centrifugal terms in the kinetic energy into a scalar electrostatic potential that augments the usual Coulombic terms. The net potential obtained in this unconventional classical limit appears to provide, via analysis of its symmetry breaking properties, a reliable heuristic model for electronic phase transitions.

For the case of collinear dissociation of the C_4^- anion, the sub-Hamiltonian for the large-D limit suggests a simple model, with a single electron in the field of four collinear atoms. We find that this model exhibits symmetry breaking analogous to both a first order and a continuous phase transition. Likewise, the model displays aspects akin to the charge redistribution seen during dissociation of the H_2^+ molecular ion.[49]

ACKNOWLEDGMENTS

We are grateful for support of this work by the National Science Foundation and a Petroleum Research grant from the American Chemical Society.

[1] M. Janssen, *Fluctuations and Localization in Mesoscopic Electronic Systems* (World Scientific, New Jersey, 2001).
[2] P. W. Anderson, Phys. Rev. **109**, 1492 (1958).
[3] E. Abrahams, P. W. Anderson, D. C. Licciardello, and T. V. Ramakrishnan, Phys. Rev. Lett. **42**, 673 (1979).
[4] D. J. Thouless, Phys. Rep. **13**, 93 (1974).
[5] O. Halfpap, Ann. Phys. (N.Y.) **10**, 623 (2001).
[6] L. Santen and W. Krauth, Nature (London) **405**, 550 (2000).
[7] G. Xiong, S. D. Wang, Q. Niu, D. C. Tian, and X. R. Wang, Phys. Rev. Lett. **87**, 216802 (2001).
[8] B. Rosam, D. Meinhold, F. Loser, V. G. Lyssenko, S. Glutsch, F. Bechstedt, F. Rossi, K. Kohler, and K. Leo, Phys. Rev. Lett. **86**, 1307 (2001).
[9] M. I. Stockman, S. V. Faleev, and D. J. Bergman, Phys. Rev. Lett. **87**, 167401 (2001).
[10] J. Ringot, P. Szriftgiser, and J. C. Garreau, Phys. Rev. Lett. **85**, 2741 (2000).
[11] F. Remacle and R. D. Levine, Proc. Natl. Acad. Sci. U.S.A. **97**, 553 (2000).
[12] N. B. Zhitenev, M. Brodsky, R. C. Ashoori, L. N. Rfeiffer, and K. W. West, Science **285**, 715 (1999).
[13] A. T. Yeh, C. V. Shank, and J. K. McCusker, Science **289**, 935 (2000).
[14] J. D. Watts, J. Gauss, J. F. Stanton, and R. J. Barlett, J. Chem. Phys. **97**, 8372 (1992).
[15] M. Algranati, H. Feldman, D. Kella, E. Malkin, E. Miklazky, R. Naaman, Z. Vagar, and J. Zajfman, J. Chem. Phys. **90**, 4617 (1989).
[16] D. Kella, D. Zajfman, O. Heber, D. Majer, H. Feldman, Z. Vager, and R. Naaman, Z. Phys. D: At., Mol. Clusters **26**, 340 (1993).
[17] D. W. Arnold, S. E. Bradforth, T. N. Kitsopoulos, and D. M. Neumark, J. Chem. Phys. **95**, 8753 (1991).
[18] S. J. Blanksby, D. S. Schoder, S. Dua, J. H. Bowie, and H. Schwarz, J. Am. Chem. Soc. **122**, 7105 (2000).

[19] J. V. Ortiz, J. Chem. Phys. **99**, 6716 (1993).
[20] D. E. Bernholdt, D. H. Magers, and R. J. Bartlett, J. Chem. Phys. **89**, 3612 (1988).
[21] W. Weltner and R. J. Van Zee, Chem. Rev. **89**, 1713 (1989).
[22] A. V. Orden and R. J. Saykally, Chem. Rev. **98**, 2313 (1998).
[23] A. Dreuw and L. S. Cederbaum, Chem. Rev. **102**, 181 (2002).
[24] K. Raghavachari, Z. Phys. **12**, 61 (1989).
[25] H. Hogreve, J. Mol. Struct. **532**, 81 (2000).
[26] T. Sommerfeld, J. Phys. Chem. A **104**, 8806 (2000).
[27] A. Dreuw and L. S. Cederbaum, Phys. Rev. A **63**, 049904 (2000).
[28] S. N. Schauer, P. Williams, and R. N. Compton, Phys. Rev. Lett. **65**, 625 (1990).
[29] A. Le Padellec, F. Rabilloud, D. Pegg *et al.*, J. Chem. Phys. **115**, 10671 (2001).
[30] M. J. Frisch, G. W. Trucks, H. B. Schlegel *et al.*, GAUSSIAN 98, *Revision A.11.3* (Gaussian, Inc.: Pittsburgh, PA, 1998).
[31] J. Simons, J. Am. Chem. Soc. **103**, 3971 (1981).
[32] J. Simons, J. Phys. Chem. **103**, 9408 (1999).
[33] Q. Shi and S. Kais, J. Am. Chem. Soc. **124**, 11723 (2002).
[34] E. R. Davidson and W. T. Borden, J. Phys. Chem. **87**, 4783 (1983).
[35] S. R. Gwaltney and M. Head-Gordon, Phys. Chem. Chem. Phys. **3**, 4495 (2001).
[36] J. Stanton, J. Gauss, and R. J. Bartlett, J. Chem. Phys. **97**, 5554 (1992).
[37] R. D. Cohen and C. D. Sherrill, J. Chem. Phys. **114**, 8257 (2001).
[38] T. D. Crawford, E. Kraka, J. F. Stanton, and D. Cremer, J. Chem. Phys. **114**, 10638 (2001).
[39] M. R. Hoffmann, W. D. Laiding, K. S. Kim, D. J. Fox, and H. F. Schaefer, J. Chem. Phys. **80**, 338 (1984).
[40] R. Murphy, H. F. Schaefer, R. H. Nobes, L. Radom, and R. M. Pitzer, Int. Rev. Phys. Chem. **5**, 229 (1986).
[41] P. O. Lowdin, Rev. Mod. Phys. **35**, 496 (1963).
[42] S. Kais and P. Serra, Adv. Chem. Phys. **125**, 1 (2003).
[43] R. S. Mulliken, J. Chem. Phys. **23**, 1833 (1955).
[44] D. R. Herschbach, J. Chem. Phys. **84**, 838 (1993).
[45] D. D. Frantz and D. R. Herschbach, Chem. Phys. **126**, 59 (1998); J. Chem. Phys. **92**, 6668 (1990).
[46] D. R. Herschbach, J. Avery, and O. Goscinski, *Dimensional Scaling in Chemical Physics* (Kluwer, Dordrecht, 1993).
[47] P. Serra and S. Kais, Phys. Rev. Lett. **77**, 466 (1996).
[48] P. Serra and S. Kais, Chem. Phys. Lett. **260**, 302 (1996).
[49] Q. Shi, S. Kais, F. Remacle, and R. D. Levine, Chem.Phys.Chem. **2**, 434 (2001).
[50] Q. Shi and S. Kais, Int. J. Quantum Chem. **85**, 307 (2001).
[51] J. G. Loeser, *Sub-Hamiltonian Methods in New Methods in Quantum Theory*, edited by C. A. Tsipis, S. Popov, D. R. Herschbach, and J. S. Avery (Kluwer Academic, Boston, 1996).
[52] J. G. Loeser, J. H. Summerfeld, A. L. Tan, and Z. Zheng, J. Chem. Phys. **100**, 5036 (1994).
[53] M. Schafer, M. Grutter, J. Fulara, D. Forney, P. Freivogel, and J. P. Maier, Chem. Phys. Lett. **260**, 406 (1996).
[54] J. Szczepanski, M. Vala, L. N. Shen, P. A. Withey, and W. R. M. Graham, J. Phys. Chem. A **101**, 8788 (1992).